

## Evaluating Landsat Thematic Mapper spectral indices for estimating burn severity of the 2007 Peloponnese wildfires in Greece

Sander Veraverbeke<sup>A,D</sup>, Willem W. Verstraeten<sup>B</sup>, Stefaan Lhermitte<sup>C</sup>  
and Rudi Goossens<sup>A</sup>

<sup>A</sup>Department of Geography, Ghent University, Krijgslaan 281 S8, BE-9000 Ghent, Belgium.

<sup>B</sup>Department of Biosystems, Katholieke Universiteit Leuven, Willem de Croylaan 34, BE-3001 Leuven, Belgium.

<sup>C</sup>Centro de Estudios Avanzados en Zonas Aridas, Universidad de la Serena, Campus A. Bello, La Serena, Chile.

<sup>D</sup>Corresponding author. Email: sander.veraverbeke@ugent.be

**Abstract.** A vast area (more than 100 000 ha) of forest, shrubs and agricultural land burned on the Peloponnese peninsula in Greece during the 2007 summer. Three pre- and post-fire differenced Landsat Thematic Mapper (TM)-derived spectral indices were correlated with field data of burn severity for these devastating fires. These spectral indices were the Normalised Difference Vegetation Index (NDVI), the Normalised Difference Moisture Index (NDMI) and the Normalised Burn Ratio (NBR). The field data consist of 160 Geo Composite Burn Index (GeoCBI) plots. In addition, indices were evaluated in terms of optimality. The optimality statistic is a measure for the index's sensitivity to fire-induced vegetation depletion. Results show that the GeoCBI–dNBR (differenced NBR) approach yields a moderately high  $R^2 = 0.65$  whereas the correlation between field data and the differenced NDMI (dNDMI) and the differenced NDVI (dNDVI) was clearly lower (respectively  $R^2 = 0.50$  and  $R^2 = 0.46$ ). The dNBR also outperformed the dNDMI and dNDVI in terms of optimality. The resulting median dNBR optimality equalled 0.51 whereas the median dNDMI and dNDVI optimality values were respectively 0.50 and 0.40 (differences significant for  $P < 0.001$ ). However, inaccuracies observed in the spectral indices approach indicate that there is room for improvement. This could imply improved preprocessing, revised index design or alternative methods.

**Additional keywords:** fire severity, Geo Composite Burn Index, Normalised Burn Ratio, Normalised Difference Vegetation Index, optimality, spectral index.

### Introduction

Wildfires play a major role in Mediterranean-type ecosystems (MTEs) (Vázquez and Moreno 2001; Díaz-Delgado *et al.* 2004; Pausas 2004; Pausas *et al.* 2008) as they partially or completely remove the vegetation layer and affect post-fire vegetation composition, water and sediment regimes, and nutrient cycling (Kutiel and Inbar 1993). As such, they act as a natural component in vegetation succession cycles (Trabaud 1981; Capitano and Carcaillet 2008; Roder *et al.* 2008) but also potentially increase degradation processes, such as soil erosion (Thomas *et al.* 1999; Chafer 2008; Fox *et al.* 2008). Assessment of the fire impact is thus a major challenge to understand the potential degradation after fire (Kutiel and Inbar 1993; Fox *et al.* 2008) and to comprehend ecosystems' post-fire resilience (Epting and Verbyla 2005; Lentile *et al.* 2007).

The terms fire severity and burn severity are often interchangeably used (Keeley 2009), describing the amount of damage (Hammill and Bradstock 2006; González-Alonso *et al.* 2007; Chafer 2008) the physical, chemical and biological

changes (Landmann 2003; Chafer *et al.* 2004; Cocke *et al.* 2005; Stow *et al.* 2007; Lee *et al.* 2008) or the degree of alteration (Brewer *et al.* 2005; Eidenshink *et al.* 2007) that fire causes to an ecosystem. Some authors, however, suggest a clear distinction between both terms by considering the fire disturbance continuum (Jain *et al.* 2004), which addresses three different temporal fire effects phases: before, during and after the fire. In this context, fire severity quantifies the short-term fire effects in the immediate post-fire environment (Lentile *et al.* 2006) and is usually measured in an initial assessment scheme (Key and Benson 2005). As such, it mainly quantifies vegetation consumption and soil alteration. Burn severity, however, quantifies both the short- and long-term impact as it includes response processes (e.g. resprouting, delayed mortality), which is evaluated in an extended assessment (EA) that incorporates both first- and second-order effects (Lentile *et al.* 2006; Key 2006). In the present study, burn severity, defined as the absolute magnitude of environmental change caused by a fire (Key and Benson 2005), is estimated 1 year post-fire.

Several remote sensing studies have discussed the potential of satellite imagery as an alternative for extensive field sampling to quantify burn severity over large areas. These studies evaluated the use of spectral unmixing, simulation techniques and spectral indices to assess burn severity (for a comprehensive review of remote sensing techniques for burn severity assessment, see Kasischke *et al.* 2007; French *et al.* 2008). Spectral mixture analysis (Rogan and Yool 2001; Lewis *et al.* 2007; Robichaud *et al.* 2007) and simulation models (Chuvieco *et al.* 2006; De Santis and Chuvieco 2007; De Santis *et al.* 2009) have proved to provide valuable information with regards to burn severity. Spectral indices, however, are a more popular approach, mainly because of their computational and conceptual simplicity. These spectral indices are typically based on Normalised Difference Spectral Indices (NDSIs), such as the Normalised Difference Vegetation Index (NDVI) (Isaev *et al.* 2002; Chafer *et al.* 2004; Díaz-Delgado *et al.* 2004; Ruiz-Gallardo *et al.* 2004; Hammill and Bradstock 2006; Hudak *et al.* 2007) or the widely used Normalised Burn Ratio (NBR) (e.g. López García and Caselles 1991; Epting *et al.* 2005; Key and Benson 2005; Miller and Thode 2007). The NDVI combines the reflectance in the R (red) and NIR (near-infrared) spectral region and is a measure of the amount of green vegetation, whereas the NBR relates to vegetation moisture by combining the NIR with MIR (mid-infrared) reflectance. As fire effects on vegetation produce a reflectance increase in the R and MIR spectral regions and a NIR reflectance drop (Pereira *et al.* 1999), bitemporal image differencing is frequently applied on pre- and post-fire NDVI or NBR images. This results respectively in the differenced Normalised Difference Vegetation Index (dNDVI) (Chafer *et al.* 2004; Hammill and Bradstock 2006) and the differenced Normalised Burn Ratio (dNBR) (Key and Benson 2005). The advantage of these pre- and post-fire differenced indices is that they permit a clear discrimination between unburned sparsely vegetated areas and burned areas, which is difficult in monotemporal imagery (Key and Benson 2005).

A wide range of field data has been considered to validate the remotely sensed indices for estimating burn severity: percentage live trees (López García and Caselles 1991; Alleaume *et al.* 2005; Smith *et al.* 2007) or percentage tree mortality (Kushla and Ripple 1998; Isaev *et al.* 2002), basal area mortality (Chappell and Agee 1996), combustion completeness (Alleaume *et al.* 2005), changes in Leaf Area Index (LAI) (Boer *et al.* 2008) and fractional cover of several components (Kokaly *et al.* 2007; Lewis *et al.* 2007; Robichaud *et al.* 2007). However, by far the most widely used field measurement is the Composite Burn Index (CBI) (Key and Benson 2005). The CBI is a semiquantitative field sampling approach based on an expert judgement procedure, developed as an operational methodology for validating remotely sensed assessments of burn severity on a national scale in the USA as part of the FIREMON (Fire Effects Monitoring and Inventory Protocol) project. The CBI is fundamentally different to the abovementioned field approaches because in the CBI, the sample plot is considered in a holistic way. Several attributes (e.g. char height, % LAI change) of the plot are visually examined and numerically rated per ecosystem stratum (substrates, low shrubs, tall shrubs, intermediate trees and high trees). The total plot score, which is an average of the average stratum ratings, expresses the plot's burn severity.

Recently, GeoCBI, a modified version of the CBI, has been developed (De Santis and Chuvieco 2009). The main modification of the GeoCBI consists of the consideration of the fraction of coverage (FCOV, the percentage of cover with respect to the total extension of the plot) of the different vegetation strata, which results in a more consistent relation between the GeoCBI and the remotely sensed burn severity measure (De Santis and Chuvieco 2009). Knowledge about the GeoCBI–dNBR relationship recently increased for the North American boreal region (Epting *et al.* 2005; Allen and Sorbel 2008; Hall *et al.* 2008; Hoy *et al.* 2008; Murphy *et al.* 2008). However, studies that assess the empirical relationship between vegetation indices and field data in the fire-prone Mediterranean biome (De Santis and Chuvieco 2007) are underrepresented in the literature.

The dNBR approach has been questioned (Roy *et al.* 2006) as it was initially developed for detecting burned areas (López García and Caselles 1991) rather than evaluating within-burn differences in combustion completeness. To evaluate dNBR index performance, a pixel-based optimality measure originating from the spectral index theory (Verstraete and Pinty 1996), which varies between zero (not at all optimal) and one (fully optimal), has been developed (Roy *et al.* 2006). An optimal burn severity spectral index needs to be very sensitive to fire-induced vegetation changes and insensitive to perturbing factors such as atmospheric and illumination effects. Very low mean optimality values were reported using *in situ* reflectance, Landsat Enhanced Thematic Mapper plus (ETM+)- and Moderate Resolution Imaging Spectroradiometer (MODIS)-sensed data, suggesting that the dNBR approach is incapable of retrieving reliable information with regards to burn severity (Roy *et al.* 2006). However, markedly higher mean optimality measures were found for six burns in Alaska, USA (Murphy *et al.* 2008). Also, the dNBR optimality statistics were found to outperform the dNDVI optimality measures (Escuin *et al.* 2008), suggesting that the dNBR remains the most optimal NDSI for estimating burn severity.

Several authors highlight the need for an independent validation of burn severity assessments based on spectral indices for specific regions and vegetation types (Cocke *et al.* 2005; Key and Benson 2005; Lentile *et al.* 2006; Chuvieco and Kasischke 2007; Fox *et al.* 2008). As the technique is conceptually and computationally easy, burn severity maps based on spectral indices could form an important instrument for post-fire management practices in the fire-prone Mediterranean ecoregion. It is therefore our objective to evaluate different spectral indices derived from Landsat TM imagery for assessing burn severity of the large 2007 Peloponnese wildfires in Greece. This general objective is fulfilled (i) by evaluating the relationship between field data and several pre- and post-fire differenced vegetation indices, and (ii) by comparing optimality statistics of those indices.

### Study area

The area of interest is located in the Peloponnese, Greece (36°30'–38°30'N, 21°–23°E) (see Fig. 1). Elevations range between 0 and 2404 m above sea level. Hot, dry summers alternate with mild, wet winters, resulting in a typical Mediterranean climate. For the Kalamata meteorological station (37°4'N, 22°1'E), the mean annual precipitation equals 780 mm

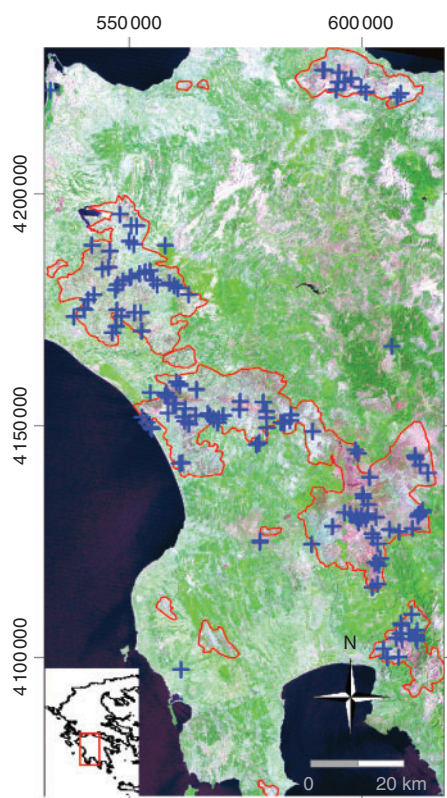


**Fig. 1.** Location of the study area and distribution of the field plots (marked by blue crosses) (Landsat TM (Thematic Mapper) image 13 August 2008, UTM (Universal Transverse Mercator) 34S ED50).

and the average annual temperature is 17.8°C (Hellenic National Meteorological Service, [www.hnms.gr](http://www.hnms.gr), accessed 29 June 2010).

Large wildfires struck the area (Gitas *et al.* 2008) in the 2007 summer. The first large burn started on 26 July 2007 and lasted until 1 September 2007. The fires devastated a large amount (more than 100 000 ha) of coniferous forest, broadleaved forest, shrublands (phrygana and maquis communities) and olive groves. Black pine (*Pinus nigra*) is the dominant conifer species. Phrygana is dwarf scrub vegetation (<1 m), which prevails on dry landforms (Polunin 1980). Maquis communities consist of sclerophyllous evergreen shrubs 2–3 m high. The shrub layer is characterised by, for example, Kermes oak (*Quercus coccifera*), Hungarian oak (*Q. frainetto*), mastic tree (*Pistacia lentiscus*), sageleaf rockrose (*Cistus salvifolius*), hairy rockrose (*C. incanus*), tree heath (*Erica arborea*) and thorny burnet (*Sarcopoterium spinosum*). The olive groves consist of *Olea europaea* trees, whereas oaks are the dominant broadleaved species.

## Methods

### Data and preprocessing

For assessing burn severity of the summer 2007 Peloponnese fires, two anniversary-date Landsat TM images (path 184, row 34) were used (23 July 2006 and 13 August 2008) (Step 1 in Fig. 2). The images were acquired in the summer, minimising effects of vegetation phenology and differing solar zenith

angles. The images were subjected to geometric, radiometric, atmospheric and topographic correction (Step 2 in Fig. 2).

The 2008 image was geometrically corrected using 34 ground control points (GCPs), recorded in the field with a Garmin eTrex Vista (Garmin International, Olathe, KS) global positioning system (GPS) (15-m error in  $x$  and  $y$  under ideal conditions (Garmin 2005), but up to 35.5 m under closed canopy (Chamberlain 2002)). The resulting Root Mean Squared Error (RMSE) was lower than 0.5 pixels. The 2006 and 2008 images were coregistered within 0.5-pixel accuracy. All images were registered in Universal Transverse Mercator (zone 34S), with ED 50 (European Datum 1950) as geodetic datum.

Raw digital numbers (DNs) were scaled to at-sensor radiance values ( $L_s$ ) (Chander *et al.* 2007) but with band-specific parameters proposed for Landsat TM data processed and distributed by the ESA (European Space Agency) (Arino *et al.*, undated). The radiance to reflectance conversion was performed using the COST method of Chavez (1996):

$$\rho_a = \frac{\pi(L_s - L_d)}{(E_o/d^2)(\cos \theta_z)^2} \quad (1)$$

where  $\rho_a$  is the atmospherically corrected reflectance at the surface;  $L_s$  is the at-sensor radiance ( $\text{W m}^{-2} \text{sr}^{-1}$ );  $L_d$  is the path radiance ( $\text{W m}^{-2} \text{sr}^{-1}$ );  $E_o$  is the solar spectral irradiance ( $\text{W m}^{-2}$ );  $d$  is the earth–sun distance (astronomical units); and  $\theta_z$  is the solar zenith angle. The COST method is a dark-object subtraction (DOS) approach that assumes 1% surface reflectance for dark objects (e.g. deep water). After applying the COST atmospheric correction, pseudo-invariant features (PIFs) such as deep water and bare soil pixels were examined in the images. No further relative normalisation between the images was required.

It was necessary to correct for different illumination effects due to topography. This was done based on the C correction method, an empirical modification of the cosine correction approach (Teillet *et al.* 1982), using a digital elevation model (DEM) and knowledge of the solar zenith and azimuth angle at the moment of image acquisition. Topographical slope and aspect data were derived from 90-m SRTM (Shuttle Radar Topography Mission) elevation data (Jarvis *et al.* 2006) resampled and coregistered with the Landsat images. The illumination is modelled as:

$$\cos \gamma_i = \cos \theta_p \cos \theta_z + \sin \theta_p \sin \theta_z \cos(\varphi_a - \varphi_o) \quad (2)$$

where  $\gamma_i$  is the incident angle (angle between the normal to the ground and the sun rays);  $\theta_p$  is the slope angle;  $\theta_z$  is the solar zenith angle;  $\varphi_a$  is the solar azimuth angle; and  $\varphi_o$  is the aspect angle. Then, terrain-corrected reflectance  $\rho_t$  is defined as:

$$\rho_t = \rho_a \left( \frac{\cos \theta_z + c_k}{\cos \gamma_i + c_k} \right) \quad (3)$$

where  $c_k$  is a band-specific parameter,  $c_k = b_k/m_k$ , where  $b_k$  and  $m_k$  are the respective intercept and slope of the regression equation  $\rho_a = b_k + m_k \cos \gamma_i$ . As topographic normalisation works better when applied separately for specific land cover types (Bishop and Colby 2002), burned area-specific C-values

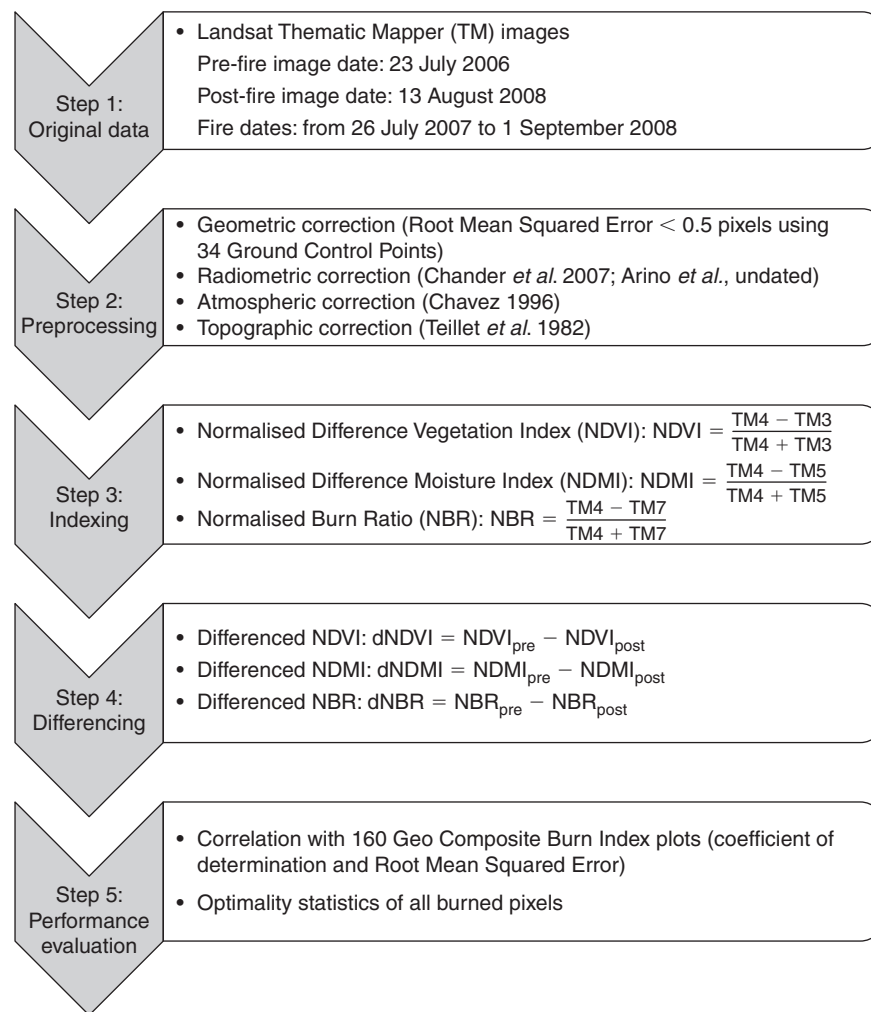


Fig. 2. Methodological workflow.

were calculated by masking the unburned areas using a two-phase threshold method (Veraverbeke *et al.* 2010).

To assess burn severity in the field, 160 GeoCBI plots were collected 1 year post-fire, in September 2008. The GeoCBI is a modified version of the CBI (De Santis and Chuvieco 2009). The GeoCBI and CBI are operational tools used in conjunction with the Landsat dNBR approach to assess burn severity in the field (Key and Benson 2005). The GeoCBI divides the ecosystem into five different strata, one for the substrates and four for vegetation layers. These strata are: (i) substrates; (ii) herbs, low shrubs and trees less than 1 m; (iii) tall shrubs and trees of 1 to 5 m; (iv) intermediate trees of 5 to 20 m; and (v) big trees higher than 20 m. The strata are grouped as understorey (i–iii) and overstorey (iv–v). In the field form, 20 different factors can be rated (e.g. soil and rock cover–colour change, % LAI change, char height) (see Table 1) but only those factors present and reliably rateable are considered. The rates are given on a continuous scale between zero and three and the resulting factor ratings are averaged per stratum. Based on these stratum averages, the GeoCBI is calculated in proportion to their

corresponding fraction of cover, resulting in a weighted average between zero and three that expresses burn severity.

The 160 sample points were selected based on a stratified sampling approach, taking into account the constraints on mainly accessibility and time, that encompasses the whole range of variation found within the burns. Contributing to this objective, 10 out of the 160 plots were measured in unburned land, with a consequent GeoCBI value of zero. The field plots consisted of 30 by 30-m squares, analogous to the Landsat pixel size. The pixel centre coordinates were recorded based on one measurement with a handheld Garmin eTrex Vista GPS device. To minimise the effect of potential misregistration, plots were at least 90 m apart and chosen in relatively homogeneous areas of at least 60 by 60 m, although preferably more (Key and Benson 2005). This homogeneity refers both to the fuel type and the fire effects. Of the 160 field plots, 67 plots were measured in shrubland, 58 in coniferous forest, 17 in broadleaved forest and 18 in olive groves. Fig. 3 shows examples of low-, moderate- and high-severity plot photographs for the coniferous forest fuel type.

**Table 1. Geo Composite Burn Index (GeoCBI) criteria used to estimate fire and burn severity in the field (after De Santis and Chuvieco 2009)**  
FCOV, fraction of cover; LAI, leaf area index

Stratum	Burn severity scale							
	No effect		Low		Moderate		High	
	0	0.5	1	1.5	2	2.5	3	
Substrates	FCOV							
Litter (l) or light fuel (lf) consumed	0%	–	50% (l)	–	100% (l)	> 80% (lf)	98% (lf)	
Duff	0%	–	Light char	–	50%	–	Consumed	
Medium or heavy fuel	0%	–	20%	–	40%	–	> 60%	
Soil and rock cover–colour	0%	–	10%	–	40%	–	> 80%	
Herbs, low shrubs and trees less than 1 m	FCOV							
Percentage foliage altered	0%	–	30%	–	80%	95%	100%	
Frequency percentage living	100%	–	90%	–	50%	< 20%	0%	
New sprouts	Abundant	–	Moderate–high	–	Moderate	–	Low–none	
Tall shrubs and trees 1 to 5 m	FCOV							
Percentage foliage altered	0%	–	20%	–	60–90%	> 95%	Branch loss	
Frequency percentage living	100%	–	90%	–	30%	< 15%	< 1%	
LAI change percentage	0%	–	15%	–	70%	90%	100%	
Intermediate trees 5 to 20 m	FCOV							
Percentage green (unaltered)	100%	–	80%	–	40%	< 10%	None	
Percentage black or brown	0%	–	20%	–	60–90%	> 95%	Branch loss	
Frequency percentage living	100%	–	90%	–	30%	< 15%	< 1%	
LAI change percentage	0%	–	15%	–	70%	90%	100%	
Char height	None	–	1.5 m	–	2.8 m	–	> 5 m	
Big trees > 20 m	FCOV							
Percentage green (unaltered)	100%	–	80%	–	50%	< 10%	None	
Percentage black or brown	0%	–	20%	–	60–90%	> 95%	Branch loss	
Frequency percentage living	100%	–	90%	–	30%	< 15%	< 1%	
LAI change percentage	0%	–	15%	–	70%	90%	100%	
Char height	None	–	1.8 m	–	4 m	–	> 7 m	

### Spectral indices and optimality

In this study, the potential of three NDSIs for assessing fire-induced vegetation change was evaluated using TM bands most sensitive to post-fire reflectance changes: TM3 (630–690 nm), TM4 (760–900 nm), TM5 (1550–1750 nm) and TM7 (2080–2350 nm). Reflectance in the visual (TM3) and MIR (TM5 and TM7) regions increases after fire, whereas the NIR region (TM4) is characterised by a reflectance drop (Pereira *et al.* 1999). To capture this information, the NDVI combines R (TM3) band with NIR (TM4) band information, whereas the Normalised Difference Moisture Index (NDMI) (Wilson and Sader 2002) and the NBR combine the NIR (TM4) band with a MIR (TM5 and TM7, respectively) band. The NBR has become the standard spectral index for assessing fire and burn severity, especially in North American regions, whereas the NDMI has not been evaluated before for fire and burn severity applications. Nevertheless, it has been suggested that TM5 is well suited for remote sensing of canopy water content (Tucker 1980). Consequently, it might also reflect post-fire reflectance changes and was included in the present study. These are the formulae of the spectral indices used (Steps 3 and 4 in Fig. 2):

$$\text{NDVI} = \frac{\text{TM4} - \text{TM3}}{\text{TM4} + \text{TM3}}, \text{dNDVI} = \text{NDVI}_{\text{pre}} - \text{NDVI}_{\text{post}} \quad (4)$$

$$\text{NDMI} = \frac{\text{TM4} - \text{TM5}}{\text{TM4} + \text{TM5}}, \text{dNDMI} = \text{NDMI}_{\text{pre}} - \text{NDMI}_{\text{post}} \quad (5)$$

$$\text{NBR} = \frac{\text{TM4} - \text{TM7}}{\text{TM4} + \text{TM7}}, \text{dNBR} = \text{NBR}_{\text{pre}} - \text{NBR}_{\text{post}} \quad (6)$$

For evaluating the optimality of the bitemporal change detection, the TM4–TM3, TM4–TM5 and TM4–TM7 bispectral spaces were considered (see Fig. 4). If a spectral index is appropriate to the physical change of interest, in this case fire-induced vegetation depletion, there exists a clear relationship between the change and the direction of the displacement in the bispectral feature space (Verstraete and Pinty 1996). In an ideal scenario, a pixel's bitemporal trajectory is perpendicular to the first bisector of the Cartesian coordinate system. This is illustrated in Fig. 4 for the displacement from unburned (U) to optimally (O) sensed burned. However, in practice perturbing factors such as atmosphere and illumination decrease the index performance. For example, in Fig. 4, a pixel displaces from unburned (U) to burned (B) after fire. Here, the magnitude of change to which the index is insensitive is equal to the Euclidian distance |OB|. Thus, the observed displacement vector UB can be decomposed into the sum of



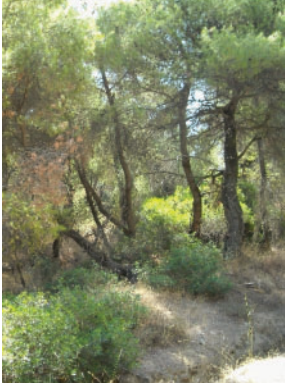
	<p>GeoCBI ratings: Understorey – 2.50 Overstorey – 3.00 Total plot – 2.65</p> <p>Large portions of downed fuels consumed. Substantial soil exposure and soil colour change. Pre-fire shrubs essentially absent and only few resprouts. Total overstorey consumption.</p>
	<p>GeoCBI ratings: Understorey – 1.06 Overstorey – 1.70 Total plot – 1.21</p> <p>Moderate char and small fuels. Most of the pre-fire herbs and shrubs exist. Some tree crowns blackened or scorched, and a substantial amount of green unaltered trees.</p>
	<p>GeoCBI ratings: Understorey – 0.56 Overstorey – 0.90 Total plot – 0.66</p> <p>Light char and little consumption of downed fuels. Most of the understorey plants remain unaltered, some shrubs show mortality. Canopy almost unaltered. Tree charring remains below 2 m.</p>

Fig. 3. Example photographs of a high-, moderate- and low-severity plot in coniferous forest.

the vectors  $UO$  and  $OB$ ; hence, the index optimality is defined as (Roy *et al.* 2006):

$$\text{Optimality} = 1 - \frac{|OB|}{|UB|} \quad (7)$$

As  $|OB|$  can never be larger than  $|UB|$ , the optimality measure varies between zero and one. If the optimality measure equals zero, then the index is completely insensitive to the change of interest. An optimality score of one means that the index performs ideally for monitoring the change of interest.

Owing to the non-linearity of the relationship between field and spectral indices estimates of burn severity (Zhu *et al.* 2006; Hall *et al.* 2008), second-degree polynomial regressions were

performed to correlate the spectral indices (independent variables) and GeoCBI field data of burn severity (dependent variables). Regression model results were compared using two goodness-of-fit measures: the coefficient of determination  $R^2$  and the RMSE. The coefficient of determination is an estimate of the proportion of the total variation in the data that is explained by the model. The RMSE is a measure of how much a response variable varies from the model predictions, expressed in the same units as the dependent data. The RMSE describes how far points diverge from the regression line. In addition, optimality statistics of all burned pixels were compared for the different indices. The median statistic was used for this purpose because of its robustness to outlier values and because the optimality distribution functions appeared to be non-normal.

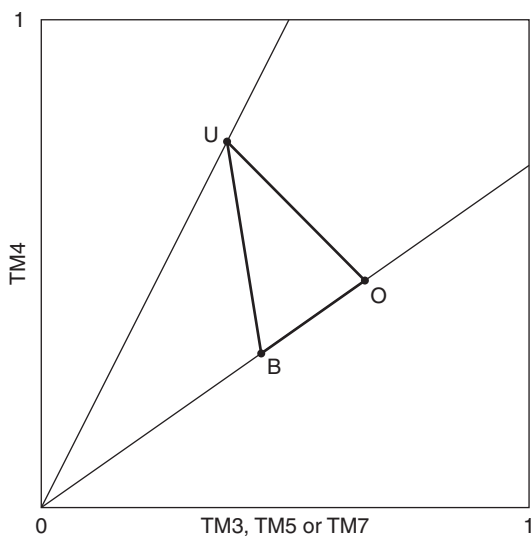


**Fig. 4.** Example pre- and post-fire trajectory of a pixel in the TM4–TM3, TM4–TM5 or TM4–TM7 feature space. A pixel displaces from unburned (U) to burned (B). O resembles the position of an optimally sensed burned pixel. The index (Normalised Difference Vegetation Index, NDVI; Normalised Difference Moisture Index, NDMI; or Normalised Burn Ratio, NBR) is sensitive to the displacement  $|UO|$  and insensitive to the displacement  $|OB|$ .

## Results

### Correlation with field data

The distribution plots and regression lines of the GeoCBI and pre- and post-fire differenced spectral indices are displayed in Figs 5*d*, 6*e* and 6*f*. Comparison of the  $R^2$  statistics shows that the GeoCBI–dNBR relationship proved to be the strongest. This relationship yielded a moderately high  $R^2 = 0.65$  for a polynomial fitting model. This was followed by the GeoCBI–dNDMI correlation, which had an  $R^2 = 0.50$ . The GeoCBI–dNDVI relationship was the weakest ( $R^2 = 0.46$ ). The decreasing trend in  $R^2$  statistic is at the same time associated with an increasing RMSE (0.35, 0.42 and 0.44 for the relationships between the GeoCBI and respectively dNBR, dNDMI and dNDVI data). The spectral index values of the dNBR approach clearly have a wider range than those of the dNDMI and dNDVI approaches. The within-burn dNBR range is almost double the within-burn dNDVI range. Most field plots have dNBR values ranging from 0 to 0.8 (see Fig. 5*f*) and dNDMI and dNDVI between 0 and 0.5 (see Fig. 5*d*, *e*). Fig. 5*a–c* depicts the respective dNDVI, dNDMI and dNBR maps. The dNBR map clearly reveals more contrast in the burnt areas than the other maps.

### Index optimality

Fig. 6*a–c* depicts the dNDVI, dNDMI and dNBR optimality maps of the burned areas. The dNBR index (median = 0.51) outperformed the dNDMI and dNDVI indices (medians of respectively 0.50 and 0.40), whereas the dNDMI provided better results than the dNDVI. The performance differences are also reflected when the respective histograms are inspected (see Fig. 6*d–f*). A large number of pixels have a dNDVI optimality lower than 0.1 and the number of pixels steadily decreased with

increasing dNDVI optimality. The dNDMI histogram is more equally distributed. Although many pixels have dNBR optimality scores above 0.2–0.4, we can observe a slightly increasing trend in terms of number of pixels when dNBR optimality increases. According to the non-parametric Wilcoxon test (Hollander and Wolfe 1999), differences in median optimality and distribution functions are statistically significant ( $P < 0.001$ ).

## Discussion

The dNBR approach gave the overall best correlation with GeoCBI field data, followed by the dNDMI and the dNDVI approach. Indices with a MIR spectral band yielded better results than indices lacking a MIR band. This corroborates with earlier research findings: AVHRR (Advanced Very High Resolution Radiometer) spectral indices based on the NIR and MIR channels had a higher discriminatory potential for burned surface mapping than indices based on the NIR and R channels (Pereira 1999); the importance of the MIR region for burned shrub–savannah discrimination with MODIS data has been demonstrated (Trigg and Flasse 2001), and significant post-fire spectral changes occurred in the 1500–2500-nm region using hyperspectral AVIRIS (Airborne Visible and Infrared Imaging Spectroradiometer) data (van Wagtenonk *et al.* 2004). In previous studies assessing the correlation between several spectral indices and CBI field data, the NBR was ranked as the best index in pre- and post-burn approaches (Epting *et al.* 2005). For fires in several regions in the USA, dNBR yielded higher correlations than dNDVI (Zhu *et al.* 2006). In the report of Zhu *et al.* the within-burn range of dNDVI values was approximately half the within-burn range of dNBR values, which is similar to our results. They also concluded that dNDVI was more influenced by hazy remote sensing conditions due to the elevated potential of atmospheric scattering in the red spectral region. Overall results show a moderately high correlation between GeoCBI field data and dNBR for the present case study in a Mediterranean environment. Polynomial fitting models resulted in  $R^2 = 0.65$ . This outcome falls within the range of results of previous studies (French *et al.* 2008).

In studies based on the spectral index theory, the dNBR had a higher mean optimality (0.49) than the dNDVI (0.18) based on Landsat TM/ETM+ images (Escuin *et al.* 2008). Our results approximate to the values reported in similar studies of 0.49 (Escuin *et al.* 2008) and ranging from 0.26 to 0.8 for six burns in Alaska, USA (Murphy *et al.* 2008). However, results contrast with the very low mean dNBR optimality scores (0.1) based on Landsat ETM+ imagery for African savannah burns (Roy *et al.* 2006). These authors also report low dNBR optimality values for MODIS-sensed fires in other ecosystems (Russia, Australia and South America). These results suggest that the dNBR index is to a high degree suboptimal for assessing burn severity. These poor optimality results, however, can possibly be explained by the fact that Roy *et al.* (2006) included unburned pixels in their optimality analysis. Unaffected pixels are generally associated with low optimality scores as a pixel's displacement in the bispectral space is only due to the noise (Escuin *et al.* 2008). This explains the low optimality values reported (Roy *et al.* 2006).

The NDMI based approach, which had not been evaluated before for estimating burn severity, performed better than the

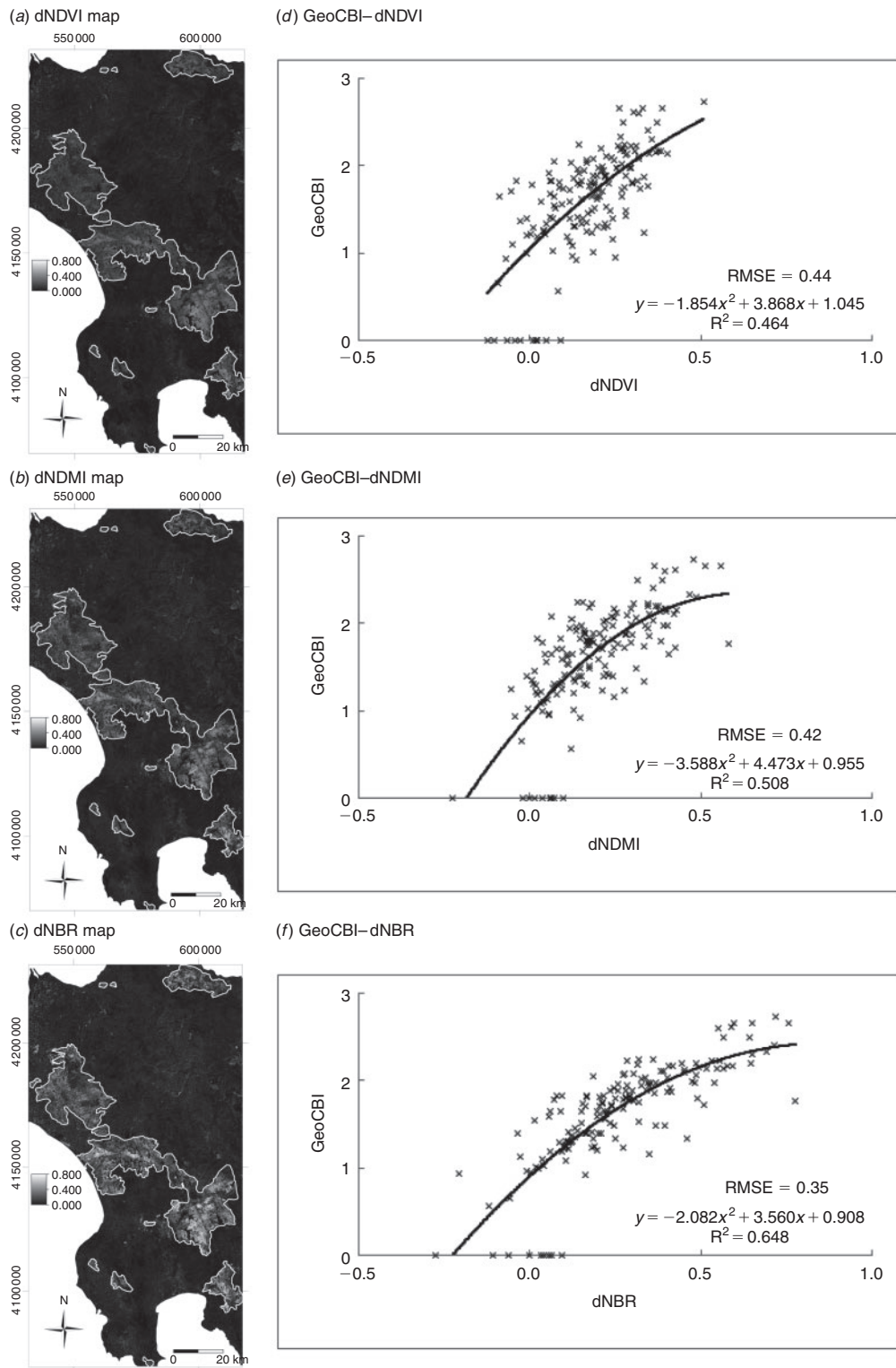


**Fig. 5.** Differenced Normalised Difference Vegetation Index (dNDVI), differenced Normalised Difference Moisture Index (dNDMI), and differenced Normalised Burn Ratio (dNBR) maps (a, b and c) and scatter plots and regression lines for the GeoCBI (Geo Composite Burn Index)–dNDVI (d), GeoCBI–dNDMI (e) and GeoCBI–dNBR (f) relationships.



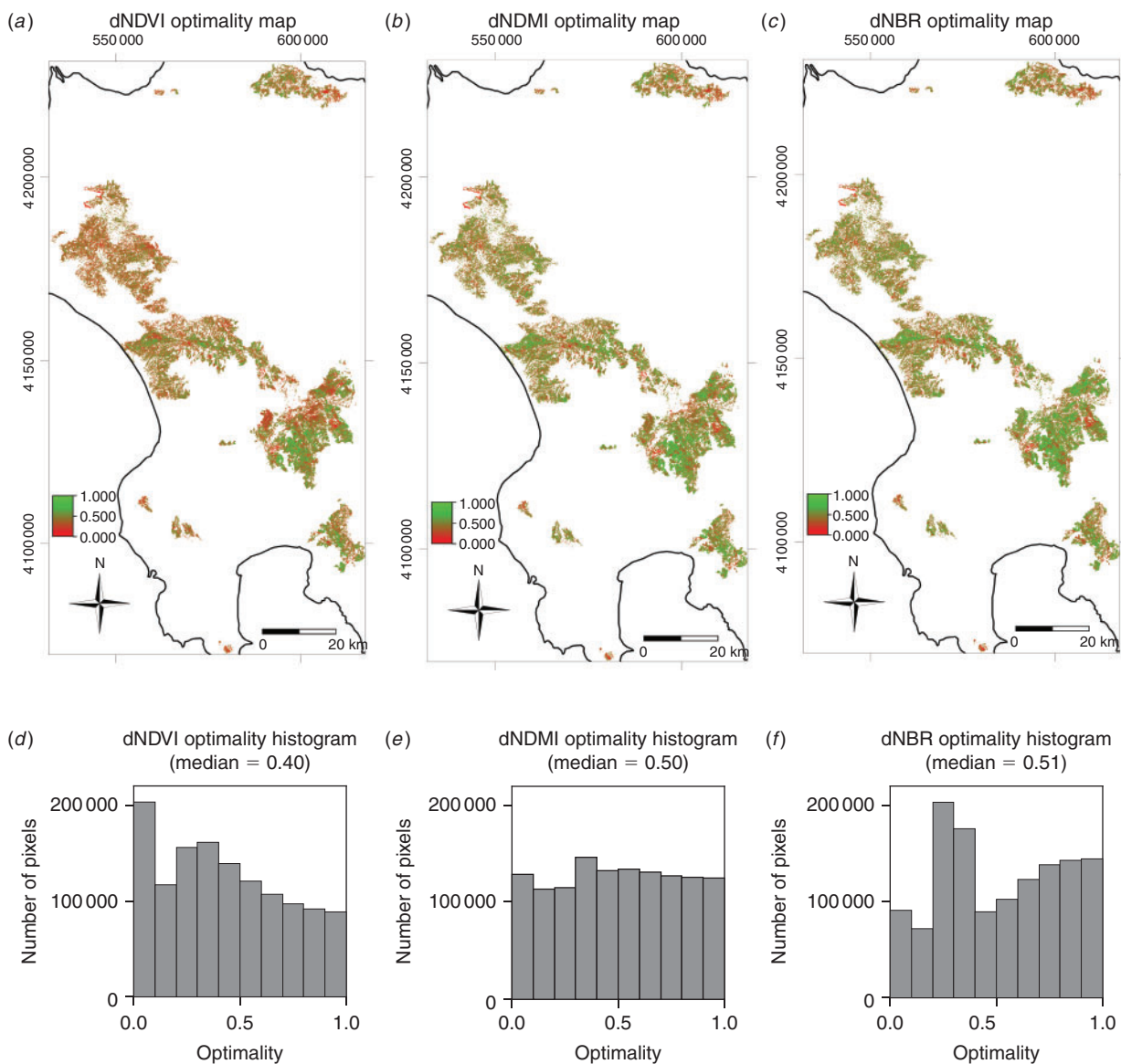


**Fig. 6.** Differenced Normalised Difference Vegetation Index (dNDVI) (*a* and *d*), differenced Normalised Difference Moisture Index (dNDMI) (*b* and *e*), and differenced Normalised Burn Ratio (dNBR) (*c* and *f*) optimality maps and histograms.

NDVI-based approach. However, the NBR outperformed the NDMI. This can be explained by the typically lower prefire reflectances in Landsat TM band 7 (2080–2350 nm) than in Landsat TM band 5 (1550–1750 nm) due to a higher degree of water absorption by vegetation at longer wavelengths. Therefore, fire-induced reflectance increase is likely to be clearer in TM7 than in TM5. As a result, an index with TM7 instead of TM5 is able to capture a larger range of variation in post-fire effects.

Apart from the fact that the dNBR outperformed the dNDMI and dNDVI, use of the dNBR to indicate burn severity is still problematic. When the GeoCBI–dNBR scatter plot and regression line (see Fig. 5*f*) are examined, three points of defectiveness attract attention: (i) the insensitivity of the regression model to unburned pixels; (ii) the saturation of the model for GeoCBI

values higher than  $\sim 2.5$ ; and (iii) the moderately high dispersion of the point cloud around the fitting line. First, the regression line crosses the  $x$  axis at  $\text{dNBR} = -0.23$ , whereas the unburned reference plots are situated closer to  $\text{dNBR} = 0$ . According to the regression equation (see Fig. 5*f*), an unburned plot with a dNBR value of zero would be associated with a GeoCBI value of 0.91, which is a clear overestimation of severity. Second, the regression model reveals asymptotic behaviour for GeoCBI values higher than 2.5. As a consequence, the empirical model potentially underestimates high-severity plots and is not able to differentiate between them. This phenomenon was also reported in previous studies (e.g. van Wagtenonk *et al.* 2004; Epting *et al.* 2005). As a solution for the insensitivity to unburned pixels and the saturation problem, a non-linear model based on

a saturated growth model was proposed (Hall *et al.* 2008). This model effectively handled the insensitivity and saturation problems, however at the expense of a lower  $R^2$  and a higher RMSE. Third, the GeoCBI–dNBR model has a RMSE of 0.35, which is approximately one ninth of the total GeoCBI variation. The observed GeoCBI values thus substantially diverge from the model predictions.

Potential sources of inaccuracy arise from both the field and satellite levels. For example, 67 GeoCBI plots were measured in shrubland to fulfil the need for a stratified sampling approach that requires that the number of plots of each fuel type is in proportion to the total area burned of each prefire land-cover type. However, as is known (e.g. van Wagtenonk *et al.* 2004; Epting *et al.* 2005), the CBI approach underperforms in non-forested areas. Part of the observed inaccuracy can also be explained by the fact that both field and satellite data are imperfect proxies of burn severity. The CBI is based on a semi-quantitative judgement procedure and therefore possibly lacks absoluteness, while several noise factors hamper satellite image analysis.

The amount of noise in the dNBR approach appeared to be fairly high, as the median dNBR optimality of 0.51 is considerably lower than the optimality of 1. An important part of the spectral change in the TM4–TM7 bispectral space occurs parallel to the NBR isolines (cf. distance |OB| in Fig. 4). Deficient preprocessing (no or unsatisfactory atmospheric correction, topographic correction, image-to-image normalisation...) can introduce noise in a remote sensing analysis. The application of these procedures in burn severity applications is sometimes blurred (French *et al.* 2008), although its importance has already been demonstrated, for example by revealing the effect of illumination on index values (Verbyla *et al.* 2008).

These findings can direct the burn severity research in different directions. First, a thorough review of the influence of preprocessing steps (especially atmospheric and topographic correction) on dNBR performance is suggested. Second, it is desired to improve the index design towards an index whose isolines are oriented to realise a higher degree of sensitivity to burn severity while providing insensitivity to other sources of spectral variation. These first two research directions retain the conceptual ease of the spectral indices approach. A third alternative could focus on the further development of more advanced remote sensing techniques for operational use. In this context, radiative transfer models (Chuvieco *et al.* 2006; De Santis and Chuvieco 2007; De Santis *et al.* 2009) and spectral mixture analysis (Lewis *et al.* 2007) have already proved to have great potential.

## Conclusions

Results of the field data and optimality-based analyses confirm one another, demonstrating that the dNBR approach was the best index of the three spectral indices tested for estimating burn severity in this case study in a Mediterranean environment. Results, however, also indicate that the dNBR approach suffers from some striking inaccuracies. The empirical fit between field and remotely sensed data is a subject for improvement, while the mean dNBR optimality score was markedly lower than the ideal scenario with optimality values of one. Further research in burn severity mapping should therefore focus on (i) noise removal

(e.g. by improved preprocessing); (ii) improved index design; and (iii) alternative methods such as radiative transfer models and spectral unmixing.

## Acknowledgements

The study was financed by the Ghent University special research funds (BOF: Bijzonder Onderzoeksfonds). The authors thank the reviewers for their constructive remarks.

## References

- Alleaume S, Hely C, Le Roux J, Korontzi S, Swap R, Shugart H, Justice C (2005) Using MODIS to evaluate heterogeneity of biomass burning in southern African savannahs: a case study. *International Journal of Remote Sensing* **26**, 4219–4237. doi:10.1080/01431160500113492
- Allen J, Sorbel B (2008) Assessing the differenced Normalized Burn Ratio's ability to map burn severity in the boreal forest and tundra ecosystems of Alaska's national parks. *International Journal of Wildland Fire* **17**, 463–475. doi:10.1071/WF08034
- Arino O, Brockman C, Veraini B, Pittella G (undated) ESA products and processing algorithms for Landsat TM. Available at <http://earth.esa.int/ers/sysutil/008e3.html> [Verified 4 July 2009]
- Bishop M, Colby J (2002) Anisotropic reflectance correction of SPOT-3 HRV imagery. *International Journal of Remote Sensing* **23**, 2125–2131. doi:10.1080/01431160110097231
- Boer M, MacFarlane C, Norris J, Sadler R, Wallace J, Grierson P (2008) Mapping burned areas and burn severity patterns in SW Australian eucalypt forest using remotely sensed changes in leaf area index. *Remote Sensing of Environment* **112**, 4358–4369. doi:10.1016/J.RSE.2008.08.005
- Brewer K, Winne C, Redmond R, Opitz D, Mangrich M (2005) Classifying and mapping wildfire severity: a comparison of methods. *Photogrammetric Engineering and Remote Sensing* **71**, 1311–1320.
- Capitaino R, Carcaillet C (2008) Post-fire Mediterranean vegetation dynamics and diversity: a discussion of succession models. *Forest Ecology and Management* **255**, 431–439. doi:10.1016/J.FORECO.2007.09.010
- Chafer C (2008) A comparison of fire severity measures: an Australian example and implications for predicting major areas of soil erosion. *Catena* **74**, 235–245. doi:10.1016/J.CATENA.2007.12.005
- Chafer C, Noonan M, Magnaught E (2004) The post-fire measurement of fire severity and intensity in the Christmas 2001 Sydney wildfires. *International Journal of Wildland Fire* **13**, 227–240. doi:10.1071/WF03041
- Chamberlain K (2002) Preliminary results for Garmin eTrex, Garmin GPS III with CSI Differential Correction (real time), Magellan Meridian Platinum at Clackamas River, OR. Available at <http://www.fs.fed.us/database/gps/mtdcrept/index.htm> [Verified 11 November 2009]
- Chander G, Markham L, Barsi J (2007) Revised Landsat-5 Thematic Mapper radiometric calibration. *IEEE Geoscience and Remote Sensing Letters* **4**, 490–494. doi:10.1109/LGRS.2007.898285
- Chappell C, Agee J (1996) Fire severity and tree seedling establishment in *Abies magnifica* forests, Southern Cascades, Oregon. *Ecological Applications* **6**, 628–640. doi:10.2307/2269397
- Chavez P (1996) Image-based atmospheric corrections – revisited and improved. *Photogrammetric Engineering and Remote Sensing* **62**, 1025–1036.
- Chuvieco E, Kasischke E (2007) Remote sensing information for fire management and fire effects assessment. *Journal of Geophysical Research* **112**, G01S90. doi:10.1029/2006JG000230
- Chuvieco E, Riano D, Danson F, Martin P (2006) Use of a radiative transfer model to simulate the post-fire spectral response to burn severity. *Journal of Geophysical Research* **111**, G04S09. doi:10.1029/2005JG000143
- Cocke A, Fule P, Crouse J (2005) Comparison of burn severity assessments using Differenced Normalized Burn Ratio and ground data. *International Journal of Wildland Fire* **14**, 189–198. doi:10.1071/WF04010

- De Santis A, Chuvieco E (2007) Burn severity estimation from remotely sensed data: performance of simulation versus empirical models. *Remote Sensing of Environment* **108**, 422–435. doi:10.1016/J.RSE.2006.11.022
- De Santis A, Chuvieco E (2009) GeoCBI: a modified version of the Composite Burn Index for the initial assessment of the short-term burn severity from remotely sensed data. *Remote Sensing of Environment* **113**, 554–562. doi:10.1016/J.RSE.2008.10.011
- De Santis A, Chuvieco E, Vaughan P (2009) Short-term assessment of burn severity using the inversion of PROSPECT and GeoSail models. *Remote Sensing of Environment* **113**, 126–136. doi:10.1016/J.RSE.2008.08.008
- Díaz-Delgado R, Lloret F, Pons X (2004) Spatial patterns of fire occurrence in Catalonia. *Landscape Ecology* **19**, 731–745. doi:10.1007/S10980-005-0183-1
- Eidenshink J, Schwind B, Brewer K, Zhu Z, Quayle B, Howard S (2007) A project for monitoring trends in burn severity. *Fire Ecology* **3**, 3–21. doi:10.4996/FIREECOLOGY.0301003
- Epting J, Verbyla D (2005) Landscape-level interactions of prefire vegetation, burn severity, and post-fire vegetation over a 16-year period in interior Alaska. *Canadian Journal of Forest Research* **35**, 1367–1377. doi:10.1139/X05-060
- Epting J, Verbyla D, Sorbel B (2005) Evaluation of remotely sensed indices for assessing burn severity in interior Alaska using Landsat TM and ETM+. *Remote Sensing of Environment* **96**, 328–339. doi:10.1016/J.RSE.2005.03.002
- Escuin S, Navarro R, Fernandez P (2008) Fire severity assessment by using NBR (Normalized Burn Ratio) and NDVI (Normalized Difference Vegetation Index) derived from LANDSAT TM/ETM images. *International Journal of Remote Sensing* **29**, 1053–1073. doi:10.1080/01431160701281072
- Fox D, Maselli F, Carrega P (2008) Using SPOT images and field sampling to map burn severity and vegetation factors affecting post-forest fire erosion risk. *Catena* **75**, 326–335. doi:10.1016/J.CATENA.2008.08.001
- French N, Kasischke E, Hall R, Murphy K, Verbyla D, Hoy E, Allen J (2008) Using Landsat data to assess fire and burn severity in the North American boreal forest region: an overview and summary of results. *International Journal of Wildland Fire* **17**, 443–462. doi:10.1071/WF08007
- Garmin (2005) Garmin eTrex Vista personal navigator. Owner's manual and reference guide. Available at <https://buy.garmin.com/shop/store/manual.jsp?product=010-00243-00&cID=167&pID=163> [Verified 11 November 2009]
- Gitas I, Polychronaki A, Katagis T, Mallinis G (2008) Contribution of remote sensing to disaster management activities: a case study of the large fires in the Peloponnese, Greece. *International Journal of Remote Sensing* **29**, 1847–1853. doi:10.1080/01431160701874553
- González-Alonso F, Merino-De-Miguel S, Roldan-Zamarron S, Garcia-Gigorro S, Cuevas J (2007) MERIS full resolution data for mapping level-of-damage caused by forest fires: the Valencia de Alcántara event in August 2003. *International Journal of Remote Sensing* **28**, 797–809. doi:10.1080/01431160600979115
- Hall R, Freeburn J, de Groot W, Pritchard J, Lynham T, Landry R (2008) Remote sensing of burn severity: experience from western Canada boreal fires. *International Journal of Wildland Fire* **17**, 476–489. doi:10.1071/WF08013
- Hammill K, Bradstock R (2006) Remote sensing of fire severity in the Blue Mountains: influence of vegetation type and inferring fire intensity. *International Journal of Wildland Fire* **15**, 213–226. doi:10.1071/WF05051
- Hollander M, Wolfe D (1999) 'Non-Parametric Statistical Methods.' (Wiley: New York)
- Hoy E, French N, Turetsky M, Trigg S, Kasischke E (2008) Evaluating the potential of Landsat TM/ETM+ imagery for assessing fire severity in Alaskan black spruce forest. *International Journal of Wildland Fire* **17**, 500–514. doi:10.1071/WF08107
- Hudak A, Morgan P, Bobbitt M, Smith A, Lewis S, Lentile L, Robichaud P, Clark J, McKinley R (2007) The relationship of multispectral satellite imagery to immediate fire effects. *Fire Ecology* **3**, 64–90. doi:10.4996/FIREECOLOGY.0301064
- Isaev A, Korovin G, Bartalev S, Ershov D, Janetos A, Kasischke E, Shugart H, French N, Orlick B, Murphy T (2002) Using remote sensing to assess Russian forest fire carbon emissions. *Climatic Change* **55**, 235–249. doi:10.1023/A:1020221123884
- Jain T, Pilliod D, Graham R (2004) Tongue-tied. *Wildfire* **4**, 22–26.
- Jarvis A, Reuter H, Nelson A, Guevara E (2006) Hole-filled seamless SRTM data V3. Available at <http://srtm.csi.cgiar.org> [Verified 4 July 2009]
- Kasischke E, Hoy E, French N, Turetsky M (2007). Post-fire evaluation of the effects of fire on the environment using remotely sensed data. In 'Proceedings of the 6th international workshop of the EARSel special interest group on forest fires. Advances in remote sensing and GIS applications in forest fire management. Towards an operational use of remote sensing in forest fire management', 27–29 September 2007, Thessaloniki, Greece. (Eds I Gitas, C Carmona-Moreno) pp. 34–52. (Office for Official Publications of the European Communities: Luxembourg)
- Keeley J (2009) Fire intensity, fire severity and burn severity: a brief review and suggested usage. *International Journal of Wildland Fire* **18**, 116–126. doi:10.1071/WF07049
- Key C (2006) Ecological and sampling constraints on defining landscape fire severity. *Fire Ecology* **2**, 34–59. doi:10.4996/FIREECOLOGY.0202034
- Key C, Benson N (2005) Landscape assessment: ground measure of severity; the Composite Burn Index, and remote sensing of severity, the Normalized Burn Index. In 'FIREMON: Fire Effects Monitoring and Inventory System'. (Eds D Lutes, R Keane, J Caratti, C Key, N Benson, S Sutherland, L Grangi) USDA Forest Service, Rocky Mountain Research Station, General Technical Report RMRS-GTR-164-CD LA, pp. 1–51. (Fort Collins, CO)
- Kokaly R, Rockwell B, Haire S, King T (2007) Characterization of post-fire surface cover soils, and burn severity at the Cerro Grande Fire, New Mexico, using hyperspectral and multispectral remote sensing. *Remote Sensing of Environment* **106**, 305–325. doi:10.1016/J.RSE.2006.08.006
- Kushla J, Ripple W (1998) Assessing wildfire effects with Landsat Thematic Mapper data. *International Journal of Remote Sensing* **19**, 2493–2507. doi:10.1080/014311698214587
- Kutiel P, Inbar M (1993) Fire impacts on soil nutrients and soil erosion in a Mediterranean pine forest plantation. *Catena* **20**, 129–139. doi:10.1016/0341-8162(93)90033-L
- Landmann T (2003) Characterizing subpixel Landsat ETM+ fire severity on experimental fire in the Kruger National Park, South Africa. *South African Journal of Science* **99**, 357–359.
- Lee B, Kim S, Chung J, Park P (2008) Estimation of fire severity by use of Landsat TM images and its relevance to vegetation and topography in the 2000 Samcheok forest fire. *Journal of Forest Research* **13**, 197–204. doi:10.1007/S10310-008-0072-X
- Lentile L, Holden Z, Smith A, Falkowski M, Hudak A, Morgan P, Lewis S, Gessler P, Benson N (2006) Remote sensing techniques to assess active fire characteristics and post-fire effects. *International Journal of Wildland Fire* **15**, 319–345. doi:10.1071/WF05097
- Lentile L, Morgan P, Hudak A, Bobbitt M, Lewis S, Smith A, Robichaud P (2007) Post-fire burn severity and vegetation response following eight large wildfires across the western United States. *Fire Ecology* **3**, 91–108. doi:10.4996/FIREECOLOGY.0301091
- Lewis S, Lentile L, Hudak A, Robichaud P, Morgan P, Bobbitt M (2007) Mapping ground cover using hyperspectral remote sensing after the 2003 Simi and Old wildfires in Southern California. *Fire Ecology* **3**, 109–128. doi:10.4996/FIREECOLOGY.0301109
- López García M, Caselles V (1991) Mapping burns and natural reforestation using Thematic Mapper data. *Geocarto International* **6**, 31–37. doi:10.1080/10106049109354290

- Miller J, Thode A (2007) Quantifying burn severity in a heterogeneous landscape with a relative version of the delta Normalized Burn Ratio (dNBR). *Remote Sensing of Environment* **109**, 66–80. doi:10.1016/J.RSE.2006.12.006
- Murphy K, Reynolds J, Koltun J (2008) Evaluating the ability of the differenced Normalized Burn Ratio (dNBR) to predict ecologically significant burn severity in Alaskan boreal forests. *International Journal of Wildland Fire* **17**, 490–499. doi:10.1071/WF08050
- Pausas J (2004) Changes in fire and climate in the eastern Iberian peninsula (Mediterranean Basin). *Climatic Change* **63**, 337–350. doi:10.1023/B:CLIM.0000018508.94901.9C
- Pausas J, Llovet J, Rodrigo A, Vallejo R (2008) Are wildfires a disaster in the Mediterranean basin? – A review. *International Journal of Wildland Fire* **17**, 713–723. doi:10.1071/WF07151
- Pereira J (1999) A comparative evaluation of NOAA-AVHRR Vegetation Indexes for burned surface detection and mapping. *IEEE Transactions on Geoscience and Remote Sensing* **37**, 217–226. doi:10.1109/36.739156
- Pereira J, Sa A, Sousa A, Silva J, Santos T, Carreiras J (1999). Spectral characterization and discrimination of burnt areas. In ‘Remote Sensing of Large Wildfires in the European Mediterranean Basin’. (Ed. E Chuvieco) pp. 123–138. (Springer-Verlag: Berlin)
- Polunin O (1980) ‘Flowers of Greece and the Balkans. A Field Guide.’ (Oxford University Press: Oxford, UK)
- Robichaud P, Lewis S, Laes D, Hudak A, Kokaly R, Zamudio J (2007) Post-fire soil burn severity mapping with hyperspectral image unmixing. *Remote Sensing of Environment* **108**, 467–480. doi:10.1016/J.RSE.2006.11.027
- Roder A, Hill J, Duguay B, Alloza J, Vallejo R (2008) Using long time series of Landsat data to monitor fire events and post-fire dynamics and identify driving factors. A case study in the Ayora region (eastern Spain). *Remote Sensing of Environment* **112**, 259–273. doi:10.1016/J.RSE.2007.05.001
- Rogan J, Yool S (2001) Mapping fire-induced vegetation depletion in the Peloncillo Mountains, Arizona and New Mexico. *International Journal of Remote Sensing* **16**, 3101–3121.
- Roy D, Boschetti L, Trigg S (2006) Remote sensing of fire severity: assessing the performance of the Normalized Burn Ratio. *IEEE Transactions on Geoscience and Remote Sensing* **3**, 112–116. doi:10.1109/LGRS.2005.858485
- Ruiz-Gallardo J, Castano S, Calera A (2004) Application of remote sensing and GIS to locate priority intervention areas after wildland fires in Mediterranean systems: a case study from south-eastern Spain. *International Journal of Wildland Fire* **13**, 241–252. doi:10.1071/WF02057
- Smith A, Lentile L, Hudak A, Morgan P (2007) Evaluation of linear spectral unmixing and dNBR for predicting post-fire recovery in a North American ponderosa pine forest. *International Journal of Remote Sensing* **28**, 5159–5166. doi:10.1080/01431160701395161
- Stow D, Petersen A, Rogan J, Franklin J (2007) Mapping burn severity of Mediterranean-type vegetation using satellite multispectral data. *GIScience & Remote Sensing* **44**, 1–23. doi:10.2747/1548-1603.44.1.1
- Teillet P, Guindon B, Goodenough D (1982) On the slope-aspect correction of multispectral scanner data. *Canadian Journal of Remote Sensing* **8**, 84–106.
- Thomas J, Walsh R, Shakesby R (1999) Nutrient losses in eroded sediment after fire in eucalyptus and pine forests in the wet Mediterranean environment of northern Portugal. *Catena* **36**, 283–302. doi:10.1016/S0341-8162(99)00051-X
- Trabaud L (1981) Man and fire: impacts on Mediterranean vegetation. In ‘Mediterranean-type Shrublands’. (Eds F di Castri, D Goodall, R Specht) pp. 523–537. (Elsevier: Amsterdam)
- Trigg S, Flasse S (2001) An evaluation of different bispectral spaces for discriminating burned shrub-savannah. *International Journal of Remote Sensing* **19**, 3499–3514.
- Tucker C (1980) Remote sensing of leaf water content in the near-infrared. *Remote Sensing of Environment* **15**, 25–30.
- van Wagtenonk J, Root R, Key C (2004) Comparison of AVIRIS and Landsat ETM+ detection capabilities for burn severity. *Remote Sensing of Environment* **92**, 397–408. doi:10.1016/J.RSE.2003.12.015
- Vázquez A, Moreno J (2001) Spatial distribution of forest fires in Sierra de Gredos (Central Spain). *Forest Ecology and Management* **147**, 55–65. doi:10.1016/S0378-1127(00)00436-9
- Veraverbeke S, Lhermitte S, Verstraeten WW, Goossens R (2010) Illumination effects on the differenced Normalized Burn Ratio’s optimality for assessing fire severity. *International Journal of Applied Earth Observation and Geoinformation* **12**, 60–70. doi:10.1016/J.JAG.2009.10.004
- Verbyla D, Kasischke E, Hoy E (2008) Seasonal and topographic effects on estimating fire severity from Landsat TM/ETM+ data. *International Journal of Wildland Fire* **17**, 527–534. doi:10.1071/WF08038
- Verstraete M, Pinty B (1996) Designing optimal spectral indexes for remote sensing applications. *IEEE Transactions on Geoscience and Remote Sensing* **34**, 1254–1265. doi:10.1109/36.536541
- Wilson E, Sader S (2002) Detection of forest harvest type using multiple dates of Landsat TM imagery. *Remote Sensing of Environment* **80**, 385–396. doi:10.1016/S0034-4257(01)00318-2
- Zhu Z, Key C, Ohlen D, Benson N (2006) Evaluate sensitivities of burn-severity mapping algorithms for different ecosystems and fire histories in the United States. USDI, Final Report to the Joint Fire Science Program: Project JFSP 01–1–4–12, pp. 1–36. (Sioux Falls, SD)

Manuscript received 5 July 2009, accepted 5 December 2009